Total VOC reactivity in the planetary boundary layer
1. Estimation by a pump and probe OH experiment

Francois Jeanneret, Frank Kirchner, Alain Clappier,
Hubert van den Bergh, and Bertrand Calpini

Air Pollution Laboratory, Swiss Federal Institute of Technology, Lausanne, Switzerland

Abstract.   The reactivity of hydroxyl radical (OH) with total volatile organic compounds (VOC), $\Sigma k_{VOC}[VOC]$, is directly obtained in the planetary boundary layer (PBL). The method is based on a perturbation technique where high initial OH concentrations are created by flash photolysis of ozone and subsequent reaction of $O(^1D)$ with H_2O. Laser-induced fluorescence is used to measure the residual OH concentration at different time delays after the perturbation (<100 ms) and obtain a direct estimate of the OH lifetime τ_{OH} for different atmospheric conditions. For specific experimental conditions the transport by the wind may be neglected, and the chemical processes governing the OH decay may be expressed by a detailed box model. With a simple chemical equation derived in this paper using τ_{OH} and complementary measurements of CO, O_3, and NO_x, an in situ estimate of $\Sigma k_{VOC}[VOC]$ in the PBL is retrieved with an uncertainty of less than 20% in comparison to the detailed box model calculations. This analysis is applied to laboratory measurements with three synthetic $NO_x/VOC/O_3$ gas mixtures, and the retrieved OH lifetimes and total VOC reactivity are discussed against model predictions.
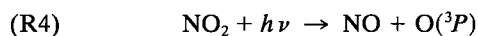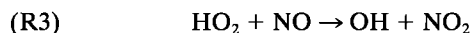
1. Introduction

Tropospheric ozone is a criteria pollutant formed by photooxidation of VOC in the presence of nitrogen oxides (NO_x = NO + NO_2) and solar radiation. In the planetary boundary layer (PBL), ozone is a major constituent of each photochemical episode [*Staffelbach et al.*, 1997] and can be harmful to both humans and vegetation [*Calpini*, 1999; *Neftel*, 1999; *Fuhrer and Bungener*, 1999]. The oxidation sequence leading to ozone production is initiated by VOC reaction with the hydroxyl radical (OH). The relative behavior of VOC and NO_x in ozone formation can be understood in terms of competition for OH. The latter participates in both the NO_x and VOC reaction cycles, thus playing a central role in the atmospheric chemistry.

Here we summarize the most important steps in this atmospheric chemistry, while the reader is referred to *Kirchner et al.* [this issue] for a detailed discussion about the complex chemical mechanism involved in the OH atmospheric chemistry at low altitude. The OH reactions with NO_x
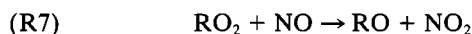
(R1) $OH + NO_2 \rightarrow HNO_3$

(R2) $OH + NO \rightarrow HONO$
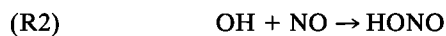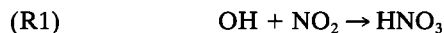
form stable products, at least temporary for HONO, and prevent the NO/NO_2 cycle leading to ozone production by the mechanism

(R3) $HO_2 + NO \rightarrow OH + NO_2$

(R4) $NO_2 + h\nu \rightarrow NO + O(^3P)$

(R5) $O(^3P) + O_2 \rightarrow O_3.$

On the other hand, the VOC oxidation by OH leads to RO_2 production, which reacts with NO to form NO_2:

(R6) $OH + VOC + [O_2] \rightarrow RO_2 + H_2O$

(R7) $RO_2 + NO \rightarrow RO + NO_2$

thus inducing the ozone production by (R4) and (R5).

At high ratios of NO_x to VOC concentration, OH will react mainly with NO_x, and at a low ratio, the VOC reactions can predominate. However, the VOC and NO_x lifetimes against the loss by reaction with OH will depend on the VOC-OH and NO_x-OH rate constants. The OH rate constants with different VOCs differ for each individual VOC species. Hundreds of different VOC species are present in the atmosphere. They may be measured independently but with VOC detection techniques that are slow and request in particular a long period of integration time.

This paper presents ideas on what we can gain with the pump and probe OH method, a method where on the contrary high-frequency measurements are possible, designed to measure in situ the OH lifetime and consequently its reactivity with the sum of all VOC present in an air parcel ($\Sigma k_{OH,VOC}[VOC]$). The latter parameter is shown to be specific to each ambient condition. Total VOC reactivity will give more significant indications on the ozone production chemistry than the VOC respective concentrations [*Kirchner et al.*, this issue]. In section 1 a summary of the experiment is presented. Section 2 underlines the effect of the transport of the pumped OH out of the probed volume by the wind. Section 3 shows how the complete atmospheric chemical mechanism can be simplified if one considers our special initial condition of a pumped OH concentration of up to 5 orders of magnitude higher than its natural concentration and analyze the OH lifetime on a timescale shorter than 20 ms. Section 4 compares the total VOC reactivity with OH predicted by box model with experimental results for three different NO_x/VOC gas mixtures.
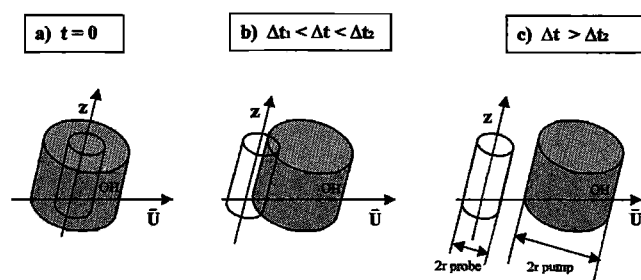
Figure 1. Pump and probe laser beams configuration: wind effects at different time delay $t_0 < t_1 < t_2$ between the pump and the probe laser beams. The pump volume is moved away from the probed LIF zone: (a) full overlap, (b) partial overlap, and (c) no overlap.

2. Pump and Probe OH Technique

Because of its high reactivity, the hydroxyl "steady state" concentration remains much below one part per trillion depending on the local chemical composition, making its detection particularly demanding. See, for example, collection of papers on the Tropospheric OH Photochemistry Experiment, Fritz Peak/Idaho Hill, Colorado, fall 1993 in *Journal of Geophysical Research*, *102*(D5), 6169–6510, 1997. [see also *Brune et al.*, 1998; *Ehhalt et al.*, 1998; *Mauldin et al.*, 1999]. Here we use a pump and probe method that makes it possible to directly measure the OH kinetics in different atmospheric conditions from remote to polluted urban air masses. It consists of creating a high initial OH concentration by flash photolysis of ozone in the Hartley band to form the excited oxygen atom $O(^1D)$, the latter reacting with water vapor to form OH. In this way, high OH concentration is initially created in the volume defined by the pump laser beam geometry. A second laser source is used for laser-induced fluorescence (LIF) detection of OH (probe beam). Thus the OH concentration is monitored at different times after the initial ozone flash photolysis, and its relaxation kinetics is followed in different environments. The pump and probe experiment was described in detail by *Calpini et al.* [1999], where it has been applied first in a reaction cell containing synthetic air at atmospheric pressure for the study of the reaction rate $k_{(OH+CH4)}$ and then in atmospheric conditions.

The pumped OH concentration is obtained using a 4th harmonic Nd:YAG laser pulse at 266 nm with an energy of up to 80 mJ/pulse and a repetition rate of 10 Hz. With a quantum yield for $O(^1D)$ in the ozone photolysis of 0.88 [*Brock and Watson*, 1980] and an ozone absorption cross section at 266 nm $\sigma_{O3}(266\ nm) = 948.5\ 10^{-20}\ cm^2$ [*Molina and Molina*, 1986], about 23% of ozone forms $O(^1D)$. The latter reacts with water vapor to form OH, but is also deactivated to $O(^3P)$ due to collisions with other air molecules or water vapor itself. Depending on the experimental conditions and the ozone and water vapor concentrations, the pumped OH concentration after the ozone flash photolysis, denoted below as $[OH]_0$ at $t = 0$, reaches typical values of up to 10^{11} molecules/cm^3.

The probe beam is generated by a frequency doubled pulsed dye laser pumped by a XeCl excimer laser. This tunable laser source is aligned on one of the most intense absorption bands of OH around 282 nm ($Q_1(2)$ transition). The fine wavelength tuning on the selected OH transition was performed initially using an intense source of OH from a methane/oxygen gas burner. The LIF signal induced by the presence of OH is directly expressed in terms of OH concentration, with an ac-

curacy of better than 30%. This overall uncertainty is the sum of the uncertainties due to the different optical parameters influencing the LIF signal (in particular, the OH absorption cross section and the quantum yield of OH fluorescence), the geometrical factors such as volume sampled for both pump and probe beams, the optical detection efficiency, and the statistical variability of the fluorescence signal. According to an experiment where a known amount of OH was produced and its absolute concentration was retrieved by this method with a relative difference of less than 6%, one may consider this 30% uncertainty as an upper limit [*Calpini et al.*, 1999].

Note that the probe wavelength itself with an energy of 0.6 mJ/pulse, a quantum yield of 0.95 [*Finlayson-Pitts and Pitts*, 1986], and an ozone absorption cross section $\sigma_{O3}(282\ nm) = 325 \times 10^{-20}\ cm^2$ [*Molina and Molina*, 1986] generates a "secondary" OH formation. For typical conditions this effect reaches a maximum secondary OH production of less than 5% with respect to $[OH]_0$. This effect is constant in time and appeared not to perturb the OH relaxation analysis at the applied conditions. A pulse box generator triggers the two lasers independently and allows controlling the time delay between the pump and the probe laser pulses.

The OH LIF is collected perpendicularly to the plane given by the gas flow and the two coaxial laser beams. The OH LIF signal is focused by a combination of two UV fused silica lenses with $f/3.5$ numerical aperture at the entrance of a double grating monochromator, and detected by a side-on photomultiplier tube.

3. Wind Effects

The time evolution of OH after the pump step is controlled by both the physical and chemical properties of the atmosphere. The atmospheric dispersion induced by diffusion and transport due to the wind blows the pumped OH out of the probed volume. This directly affects our measure of the OH time decay. As the aim of this study is to measure the atmospheric OH relaxation time in a "purely chemical" regime, the geometrical configuration of the experiment must be adapted so to avoid any wind effects, at least for a given time delay after OH was formed.

Initially, the pump laser beam creates OH in the volume defined by its direction and its cross-sectional area. The OH concentration is measured in a smaller volume delimited by the probe beam geometry as seen in Figure 1. After the ozone flash photolysis, all atmospheric species return to equilibrium because of the combined effects of the chemistry and the atmospheric dispersion. This is expressed at any time by the mass conservation equation

$$\underbrace{\partial C_k/\partial t + \nabla U C_k}_{A} = \underbrace{\nabla(\kappa \nabla C_k)}_{B} + \underbrace{\dot\omega_k}_{C} \qquad (1)$$

where

C_k concentration of the kth species;
U wind speed;
κ molecular diffusion;
$\dot\omega_k$ net chemical reaction rate for the kth species.

In this equation, term A is the transport induced by the wind, term B is the molecular diffusion, and term C contains the production and consumption of species C_k by chemical and photochemical reactions. To be allowed to neglect term A, one has to adapt the geometry of the two laser beams, as shown in

Figure 1, and to accurately control their alignment on the same axis as well as the beam divergence of the two beams. The wind transports the pumped OH volume out of the probe volume. The two beam radii r_{pump} and r_{probe} must assure a time window Δt, during which the experiment is not biased by the wind. During Δt the wind also fluctuates because of turbulent effects. Thus we have to consider U_{max} and U_{min} to be the maximum and minimum wind speed during the OH relaxation. The experimental conditions can be defined in three steps:

full overlap (Figure 1a) of the probe beam in the pumped area if $\Delta t < \Delta t_1$ with

$$\Delta t_1 = |r_{pump} - r_{probe}|/U_{max}, \qquad (2)$$

no overlap (Figure 1c) if $\Delta t > \Delta t_2$ with

$$\Delta t_2 = |r_{pump} + r_{probe}|/U_{min}, \qquad (3)$$

partial overlap (Figure 1b) if $\Delta t_1 < \Delta t < \Delta t_2$.

When the overlap is complete ($\Delta t < \Delta t_1$), the transport has no effect on the OH time decay, and term A in (1) can be neglected. The measured OH relaxation is in this case exclusively due to the chemical mechanisms and the diffusion. On the other hand, when $\Delta t > \Delta t_2$, there is no overlap, and the perturbed volume is totally out of the LIF zone in which case the air mixture in the probed volume is renewed. This condition will determine the laser frequency $f < 1/\Delta t$ of the pump and probe laser beam in order to avoid any memory effect in the pumped OH volume. Thus the beam radii and the experimental repetition rate are defined by $\Delta t < \Delta t_1$: the chemical OH decay is not biased by transport effect; and a laser frequency $f = 1/\Delta t$ where $\Delta t > \Delta t_2$ to avoid any memory effect.

For calm atmospheric condition ($U = 2$ m/s) a typical experiment will be performed with the pump and the probe radii at the experimental site set at 85 and 5 mm, respectively. This would lead to a time window $\Delta t_1 = 40$ ms where the transport would not influence the OH relaxation. In this case, no memory effect would be observed for $\Delta t_2 > 45$ ms or an experimental repetition rate typically lower than 20 Hz.

With $\Delta t < \Delta t_1$, term A in (1) is neglected:

$$\partial C_k/\partial t = \nabla(\kappa \nabla C_k) + \dot{\omega}_k. \qquad (4)$$

Because of the beam geometry, the diffusion term can be written in cylindrical coordinates:

$$\frac{\partial C_k}{\partial t} = \frac{\kappa}{r}\frac{\partial}{\partial r}\left(r\frac{\partial C_k}{\partial r}\right) + \frac{\kappa}{r^2}\frac{\partial^2 C_k}{\partial \theta^2} + \kappa\frac{\partial}{\partial z}\left(\frac{\partial C_k}{\partial z}\right) + \dot{\omega}_k \qquad (5)$$

where

r coordinate perpendicular to the pump laser beam axis;
z coordinate along the pump laser beam axis;
θ polar coordinate;
κ molecular diffusion coefficient.

Because of the beam symmetry, $\partial C_k/\partial \theta = 0$ and $\partial C_k/\partial z \ll \partial C_k/\partial r$. The diffusion along the pump beam axis can be neglected compared to the diffusion perpendicular to the axis. Thus (5) becomes

$$\frac{\partial C_k}{\partial t} = \frac{\kappa}{r}\frac{\partial}{\partial r}\left(r\frac{\partial C_k}{\partial r}\right) + \dot{\omega}_k. \qquad (6)$$

In order to check for the respective influence of the chemistry and the diffusion effects on the OH lifetime, (6) is expressed on a cylindrical coordinate grid with the diffusion terms con-

sidered as production and loss terms for the chemical solver. For time delays below 100 ms a sensitivity analysis, with and without molecular diffusion, for the OH relaxation in different atmospheric conditions, shows that this diffusion term produced rigorously no effect. Therefore

$$\partial C_k/\partial t = \dot{\omega}_k \qquad (7)$$

with the time evolution of any atmospheric species depending only on the chemical reactions. With these assumptions the pump and probe method may be used to measure the OH lifetime in a "pure chemical regime" or without transport effect. However, this also underlines that the pump and probe method is limited to the analysis of the OH time decay for short time delay only, typically below 100 ms. Section 3 will demonstrate that even under such conditions, large variations in the OH relaxation time are obtained for different atmospheric conditions and as a result the total VOC reactivity with OH can be retrieved.

4. OH Chemical Reactions in the Atmosphere

The atmospheric photochemistry is a complex mechanism including homogeneous and heterogeneous chemical reactions. This study will be restricted to the gas phase chemistry only. The chemical mechanism used in this study is the Regional Atmospheric Chemistry Mechanism (RACM) [Stockwell et al., 1997], a mechanism used to simulate the atmospheric chemical composition in the troposphere from the Earth's surface through the upper troposphere for remote to polluted urban conditions. The RACM mechanism is a further development of the RADM2 [Stockwell et al., 1990]. This lumped mechanism which was intensively tested against smog chamber experiments contains 77 chemical species among which 28 are radicals, with 234 reactions. In our case, the reactions including OH + OH were added to the original mechanism. Their importance will be discussed later.

Because of the fast OH chemistry, the numerical runs predicting the OH time decay are operated on time steps of 0.1 ms/step. The chemical solver is based on the method of Gong and Cho [1993]. It is a hybrid implicit/explicit scheme, with an explicit scheme used for species with relatively long lifetimes and the implicit Newton-Raphson iterative scheme used for the fast reacting species.

Four atmospheric conditions were used to observe the OH relaxation in different chemical regimes: (1) polluted, (2) moderately polluted, (3) rural, and (4) remote conditions. They are defined in Table 1. The NO_x concentrations and the sum of all VOC were taken from Finlayson-Pitts and Pitts [1986]. The VOC split of the polluted and moderately polluted cases were derived by taking the noontime concentrations resulting from the second day of a box model run under the conditions of the "plume" case of Kuhn et al. [1998]. This is a moderately polluted case using emissions which are representative for continental European air [Derwent and Jenkin, 1991]. The VOC split for the rural case was taken from Fehsenfeld et al. [1992]. In the remote case the VOC split resulting from Kuhn et al. [1998] was modified by increasing the percentages of biogenically emitted VOC, in particular, isoprene and terpenes. The mixing ratios are summarized in Table 1 as "initial" values for each trace gas or family and for the four chemical regimes. The simulation was performed in two steps. The initial values of Table 1 were used to initiate the box model for 20 min in order to obtain realistic mixing ratios for peroxy radicals and a real-

Table 1. Initial Conditions for Four Typical Atmospheric Cases[a]

	Polluted		Moderately		Rural		Remote	
Species	Initial	Input Before Pump	Initial	Input Before Pump	Initial	Input Before Pump	Initial	Input Before Pump
Inorganics								
O_3	50	50.8	80	84.7	72	81.3	50	48.6
H_2O_2	2	2.0	2	2.0	2	3.0	2	2.0
CO	1000	1000	200	200	200	200	200	200
H_2O	1×10^7	1×10^7	1×10^7	1×10^7	1×10^7	1×10^7	1×10^7	1×10^7
NO_x	500	493	5.0	4.1	6.0	4.7	0.10	0.036
NO	150	142	1	0.7	1	0.7	···	0.002
NO_2	350	351	4	3.4	5	4.0	0.10	0.034
Alkanes								
CH_4	1700	1700	1700	1700	1700	1700	1700	1700
NMVOC	1000	996.5	100.0	98.59	102.6	105.0	30.00	28.64
ETH (ethane)	53	53	5.3	5.3	···	···	0.53	0.53
HC3 (low-reactive alkanes)	429	428	42.9	42.2	41.7	41.6	4.29	4.28
HC5 (middle-reactive alkanes)	88	88	8.8	8.5	2.2	2.2	0.88	0.88
HC8 (high-reactive alkanes)	25	25	2.5	2.3	0.1	0.1	0.25	0.25
Alkenes								
ETE (ethene)	30	30	3.0	2.8	···	···	0.3	0.3
OLT (terminal olefines)	2	1.97	0.2	0.16	···	2.0	0.02	0.49
OLI (internal olefines)	1	0.67	0.1	0.03	···	···	0.01	0.03
ISO (isoprene)	···	···	···	···	38.5	32.0	10.00	8.96
API (α-pinene)	···	···	···	···	3.4	2.5	6.67	5.59
LIM (d-limonene)	···	···	···	···	···	···	3.33	2.14
Aromatics								
TOL (toluene)	56	56	5.6	5.4	0.5	0.5	0.56	0.56
XYL (xylene)	8	8	0.8	0.7	0.2	0.2	0.08	0.08
Carbonyls								
HCHO	60	56	6.0	5.9	1.0	5.0	0.6	0.9
ALD (higher aldehydes)	50	51	5.0	5.1	6.0	6.8	0.5	1.2
Methacrolein	···	···	···	···	···	2.7	···	0.8
KET (ketones)	198	199	19.8	20.2	9.0	9.6	1.98	2.45
Radicals								
peroxy radicals	···	5.5×10^{-4}	···	4.0×10^{-2}	···	9.4×10^{-2}	···	1.2
HO_2	···	3.0×10^{-4}	···	1.8×10^{-2}	···	2.7×10^{-2}	···	1.9×10^{-3}
RO_2	···	2.5×10^{-4}	···	2.2×10^{-2}	···	6.7×10^{-2}	···	1.2

[a]All concentrations in ppb.

istic ratio between NO and NO_2. The result (input before the pump) was then used as initial conditions for the chemistry at the time when OH is pumped in the atmosphere. This is the first time step of the pump and probe simulation with this model. The polluted atmosphere is characterized by high concentrations of pollutant precursors of nonmethane volatile organic compounds (NMVOC) and NO_x. The remote case, a fairly clean atmosphere, is composed of low precursor concentrations except for some typical OH-reactive remote hydrocarbons such as isoprene. The moderately polluted and rural conditions are cases that are similar with moderate NO_x and high biogenic VOC conditions but with different VOC split. The species acronyms of Table 1 are defined by Stockwell et al. [1997].

The natural logarithms of the absolute OH concentration time decays predicted by RACM are presented in Figure 2 on a time window of 100 ms. In this simulation the maximum initial OH concentration is about 3×10^{10} molecules/cm^3 for both the rural and moderately polluted cases since the ozone concentration was in both cases around 80 ppb as input before pump (see Table 1). In the two other cases the initial OH concentration is lower due to respectively lower initial ozone concentrations.

In the polluted condition a fast relaxation is predicted during the first 20 ms. This is due to the high concentration of NO_x, CO, and VOCs. Lower concentrations of NO_x and VOCs lead to a slower OH time decay. This is confirmed in the rural case

with a slow OH decay, and an even slower decay in the remote case. In the moderately polluted case the VOCs and NO_x concentrations are higher than in the remote case, but because of the missing high reactive biogenic VOC like isoprene, LIM, and API, the reactivity of the VOC split is much less, thus giving the slowest relaxation time. Each of the remote, rural,
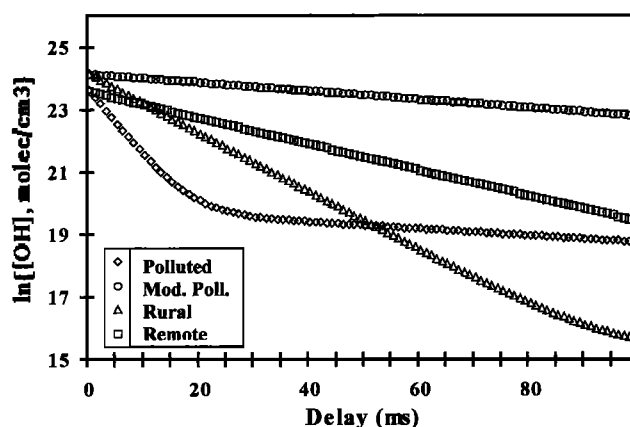

Figure 2. Natural logarithm of the predicted OH concentration decay versus time for the four atmospheric conditions defined in Table 1.

and moderately polluted cases exhibit OH time decay curves with straight-line shape until more than 80 ms. This corresponds to a pseudo first-order OH decay. For the polluted case this linear behavior is well seen for the first 20 ms, but secondary chemical processes are involved at a longer time scale. This effect as well as the importance of the absolute initial OH concentration and its implication in the accuracy of the proposed method will be discussed in more detail in the following chapter. As a preliminary indication, Figure 2 illustrates that even under such a short timescale, the OH time decay for various atmospheric conditions appears to be very different. The concentration dynamic range is higher than 2 orders of magnitude. For the OH lifetime a pseudo first-order OH time decay can be directly estimated from Figure 2. This is done by considering only the first 20 ms for the polluted case, and the result is $\tau(OH)_{polluted} = 4.85$ ms. For the three other cases this first-order OH lifetime is obtained considering the first 80 ms, and the results are $\tau(OH)_{rural} = 10.5$ ms, $\tau(OH)_{remote} = 23.5$ ms, and $\tau(OH)_{moderately\ polluted} = 75$ ms, respectively.

The result presented in Figure 2 were obtained with the complete set of reactions defined in RACM. The chemical reaction rate $\dot{\omega}_k$ in (7) can be decomposed into a production rate P_k and a loss rate L_k term:

$$\partial C_k/\partial t = P_k(t) - L_k(t)C_k. \tag{8}$$

The OH concentration produced by the pump laser being typically 4–5 orders of magnitude higher than the ambient concentration and the radical being so reactive, the decay in the short time delay is mainly due to a pure chemical removal. Therefore the relaxation would be a simple exponential. This is a first indication that the OH decay can be described in this case by a first-order loss and $P_k(t)$ can be neglected. With this hypothesis the OH time dependence would be

$$d[OH]/dt = -L_{OH}[OH] \tag{9}$$

where L_{OH} is constant in time and depends specifically upon each atmospheric condition. The solution of (9) is

$$\ln[OH]_t = \ln[OH]_0 - 1/\tau_{OH}t \tag{10}$$

where $1/\tau_{OH} = L_{OH}$ is the slope of $\ln[OH]_t$ versus time.

Let us show in which conditions the hypothesis of a production term $P_k(t) = 0$ is valid. OH is produced in the atmosphere mainly through the reactions $(HO_2 + NO)$, the photodissociation of ozone followed by the $(O(^1D) + H_2O)$ reaction, the photodissociation of nitrous acid (HONO), and the ozone-alkenes reactions, the latter being of special importance as a free radical source at dusk and during the night [Paulsen et al., 1998]. While the OH production by natural photodissociation processes and the ozone-alkenes reactions are orders of magnitude lower than the initial OH concentration generated by the experiment itself, the reaction

(R3) $HO_2 + NO \rightarrow OH + NO_2$
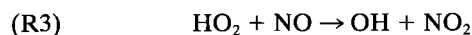
may have an influence in the OH decay because high OH concentration leads to hydroperoxyl radical HO_2 production via the photooxidation channel

(R6) $OH + VOC \rightarrow RO_2 + H_2O$

(R8) $RO_2 + NO[+ O_2] \rightarrow (HO_2$ or $R'O_2) + NO_2$

            + oxygenated VOC.
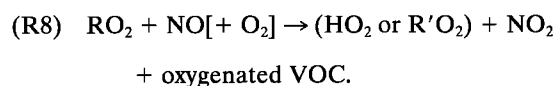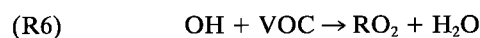
HO_2 is formed if the intermediately formed oxyradical RO reacts with O_2, and $R'O_2$ is formed if RO reacts by isomerization or decomposition. The relatively high HO_2 concentration feeds the $(HO_2 + NO)$ reaction. The latter, however, needs the presence of nitric oxide and will thus occur mainly in the polluted atmosphere. A sensitivity analysis performed with the box model using the RACM mechanism shows that the increase of OH concentration due to the total production term $P_k(t)$ is smaller than 0.5% with respect to the pumped OH concentration for time delays smaller than 100 ms for moderately polluted, remote, and rural conditions. This ratio may increase up to 10% for the polluted case and a time delay of 20 ms. Such a high OH production term in a polluted atmosphere is explained by the high VOC concentration which transforms rapidly the OH radical into HO_2, the latter reacting with NO to form OH. In this case the approximation of a negligible production term $P_k(t) = 0$ will be limited to short time delays especially for NO-rich atmosphere. This explains the result in Figure 2 for the polluted case, where for $\Delta t > 20$ ms the secondary OH production can no longer be neglected. One should also note that even if HO_2 is produced via the VOC photooxidation, the secondary reaction $(HO_2 + OH)$ only influences the OH concentration by less than 1% up to 200 ms for any of the atmospheric conditions defined in Table 1. Note that the reaction $(HO_2 + O_3)$ is too slow for being a significant OH source during the experiment. The HO_2 lifetime in regard to reaction with ozone is of the order of minutes.

Additional sensitivity runs were performed to address the question of possible interference due to reactions of OH with organic peroxy radicals (RO_2), in particular in a less polluted environment. This was done for the moderately polluted, rural, and remote conditions where the highest VOC reactive species are used as input in the model and thus where the highest RO_2 secondary reaction with OH is expected. In all cases the concentrations of the most reactive VOC, namely, the RACM species HC8, OLT, OLI, ISO, API, LIM, XYL, HCHO, ALD, and MACR with a reaction rate over 10^{-11} cm^3 molecules^{-1} s^{-1}, were more than a factor of 10 higher than the highest possible RO_2 concentration. Assuming that the rate constant of $(RO_2 + OH)$ is identical to the reaction rate of its VOC precursor with OH if it is higher than 2×10^{-11} cm^3 molecules^{-1} s^{-1} and keeping a constant value of 2×10^{-11} cm^3 molecules^{-1} s^{-1} for the other RO_2, the largest impact due to $(RO_2 + OH)$ was found in the remote case. In this case the OH lifetime predicted by RACM, τ_{RACM}, was 6% lower than without considering this reaction. This corresponds to a total VOC reactivity changed from 42.54 s^{-1} without considering the RO_2 interference to 45 s^{-1} if $(RO_2 + OH)$ is added to the RACM mechanism with the above mentioned assumptions on the respective reaction rates. This contribution is fairly low as long as the initial OH concentrations are below 10^{11} molecules/ cm^3. Thus the reactions $(OH + RO_2)$ were no longer introduced in the chemical mechanism.

The loss rate L_{OH} is a constant that depends on the concentration of all reactants with OH:

$$L_{OH} = 1/\tau_{OH} = \sum_i k_{OH,i}[C_i]_0 \tag{11}$$

where $k_{OH,i}$ is the rate constant of the OH reaction with the species i and $[C_i]_0$ is the concentration of species i at $t = 0$. Hence the RACM mechanism still does not adequately reflect
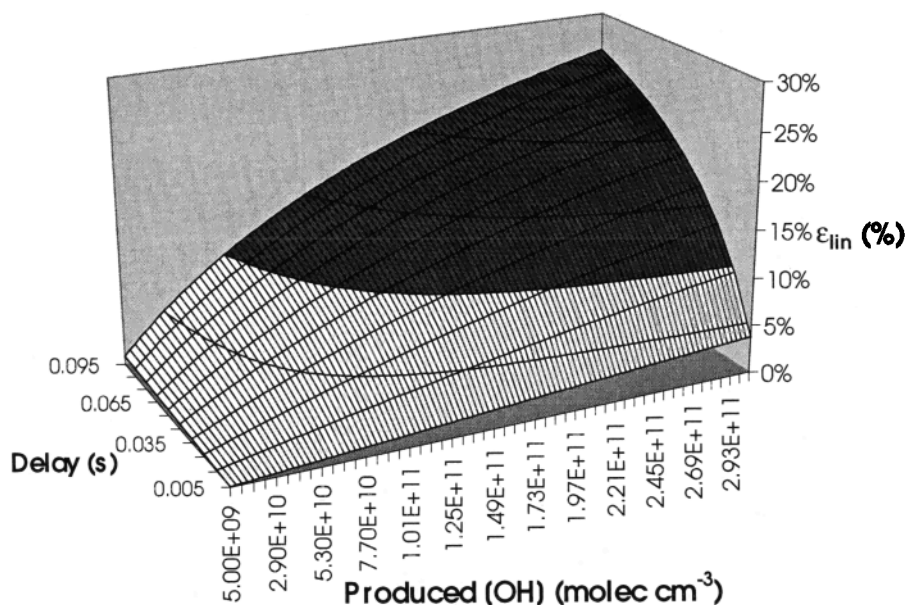
Figure 3. Linearization error ε_{lin} for different initial OH concentrations and different time delays between the pump and the probe beams for the moderately polluted condition ($L_{OH} = 10 \text{ s}^{-1}$).

the chemical mechanism involved in this pump and probe experiment without additional second-order reactions due to the high pumped OH concentrations. They correspond to the following (OH + OH) self-reactions:

(R9) $OH + OH \rightarrow O(^3P) + H_2O$

(R10) $OH + OH + M \rightarrow H_2O_2 + M$.
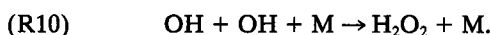
According to (11) the time-dependent OH reaction rate $2k_{OH}[OH]$ has an upper limit $2k_{OH}[OH]_0$ at time $t = 0$ that can be used as a constant approximation for short time delays. Let us define a new loss rate L' specific to the pump and probe experiment:

$$L' = L_{OH} - 2k_{OH}[OH]_0 \qquad (12)$$

and consider the validity of this approximation replacing (12) in (9) and solving explicitly (9). We obtain

$$\ln [OH] = \ln \frac{DL'}{2k_{OH}} - L't - \ln (1 - De^{L't}) \qquad (13)$$

where $D = 2k_{OH}[OH]_0/L_{OH}$ is a constant in time. Equation (13) can be developed as a Taylor's series at $t = 0$ in terms of ($L_{OH}t$):

$$\underbrace{\ln [OH](t)}_{A} = \underbrace{\ln [OH]_0 - L_{OH}t}_{B} +$$

$$\underbrace{\frac{D}{2} (L_{OH}t)^2 - \frac{D(D+1)}{6} (L_{OH}t)^3 + \frac{D(D^2+4D+1)}{24} (L_{OH}t)^4 - \cdots}_{C} \cdot$$

$$\qquad (14)$$

The solution is a straight line with a slope L_{OH} (term B) perturbed by higher-order terms (term C). Let us define ε_{lin} as the relative error if one neglects term C in (14):

$$\varepsilon_{lin} = C/A = 1 - (B/A). \qquad (15)$$

The parameter ε_{lin} is directly depending on the pumped OH concentration at $t = 0$, $[OH]_0$, and the loss rate L_{OH}. As a result of (14), the error ε_{lin} will be larger if $[OH]_0$ is higher, or if the loss rate L_{OH} is slower. In Figure 3 a sensitivity analysis of the error induced by neglecting term C in (15) is plotted versus the initial OH concentration $[OH]_0$ and the time delay of the OH measurement after the pump step. This analysis is performed for the moderately polluted case with the slowest loss rate ($L_{OH} = 10 \text{ s}^{-1}$) as shown in Figure 2, a case study where the highest error ε_{lin} is expected. The clear part in Figure 3 defines the time delay versus $[OH]_0$ with ε_{lin} smaller than 10%. For example, for $[OH]_0 < 2 \times 10^{11}$ molecules/cm^3 the maximum delay limiting ε_{lin} to less than 10% will be 25 ms. The increase of L_{OH} for remote, rural, or polluted conditions will simply lower ε_{lin}.

At this point of the study we have shown that the OH time dependence can be approximated by a first-order reaction rate if the following is assumed:

1. One may consider as negligible any OH production term. This assumption is shown not to be valid any more in highly polluted conditions where OH in the presence of high nitric oxide may generate a secondary OH production term not constant in time.

2. One may use a constant value for the OH self-reaction term in the form $2k_{OH}[OH]_0$. This simplification in the estimation of the OH lifetime generates an error of about 10% for atmospheric conditions where OH has the longest lifetime.

With these assumptions our first-order approximation is now expressed by

$$1/\tau_{OH} = \sum_i k_i[C_i]_0 + 2k_{OH}[OH]_0 \qquad (16)$$

where the contribution of the different $[C_i]_0$ representing any trace gas constituents in the atmosphere reacting with OH may have a very different effect on the OH lifetime. The product
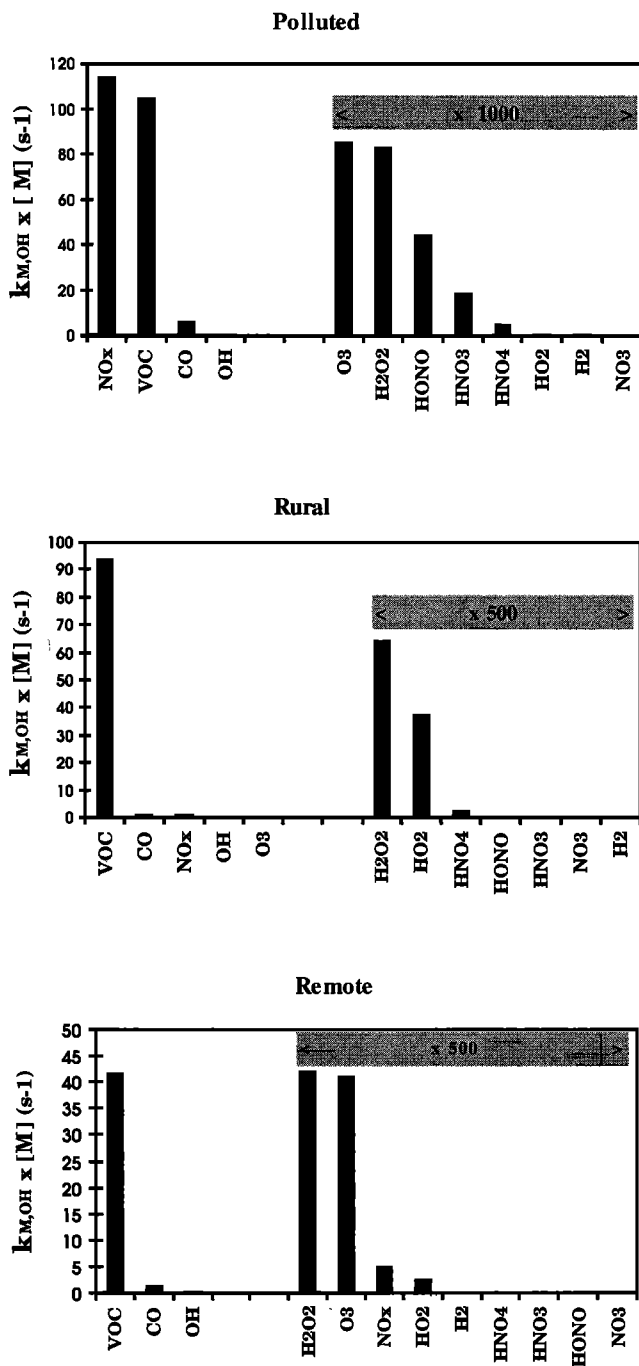
Figure 4. Species reactivity with OH at $t = 0$ for the polluted, rural, and remote atmospheric conditions defined in Table 1. Note the change in the vertical scale and the expanded scale by a factor of 1000, 500, and 500, respectively, for the less reactive species. The sum of these low-reactive species with OH contributes to less than 0.6% with respect to the overall reactivity with OH.

$k_i[C_i]_0$ is shown in Figure 4 with the concentration species defined in Table 1. Here we present for clarity only the polluted, rural, and remote cases since the moderately and rural cases are very similar except for the VOC split.

While the VOC, NO_x, OH, CO, and O_3 species are the most significant reactants with OH, in the polluted case the product $k_i[C_i]_0$ depends mainly upon the NO_x reactivity with OH, and in the two other cases the total VOC reactivity with OH dom-

inates. Note the change in the vertical scales for the three cases in Figure 4, and also the expanded scales ($\times 1000$, $\times 500$, and $\times 500$ for the polluted, rural, and remote cases, respectively). This expanded scale is used to underline the relatively low contribution of other species such as H_2O_2, HO_2, and others with respect to the main reactants with OH.

While the importance of the $[OH]_0$ was already mentioned as a possible source of error at too high concentration (see Figure 3 and associated discussion about the linearization error), (16) would also remain valid as long as the implicit assumption of constant concentration $[C_i]_0$ versus time would be verified. This assumption will be particularly sensible in the remote case where high amount of very reactive VOC species are present and may be depleted during the course of a measurement. On the basis of the box model run of the remote case, the respective concentration of isoprene, d-limonene, α-pinene, or formaldehydes and higher aldehydes (input before the pump, see Table 1) were predicted to change between $t = 0$ and $t = 20$ ms in the following way: isoprene from 8.96 ppb to 8.76 ppb, d-limonene from 5.59 ppb to 5.53 ppb, and α-pinene from 2.14 ppb to 2.06 ppb, while the other VOC species were even more stable. With the different reaction rate used in RACM, these relatively small changes in the VOC concentration did not affect the analysis of the OH lifetime, and the assumption of constant VOC concentrations was confirmed.

In Figure 4 only a small number of species are playing a significant role in their reaction with OH. Thus one may propose a further simplification consisting of keeping only the most significant species in the OH decay. The OH lifetime would then become

$$1/\tau_{OH} = \sum k_{VOC}[VOC]_0 + \sum k_{NO_x}[NO_x]_0 + k_{CO}[CO]_0$$
$$+ k_{O_3}[O_3]_0 + 2k_{OH}[OH]_0 \qquad (17)$$

where mainly the inorganic species have been cancelled out because of their weak contribution to the OH decay. The contribution of the sum of the cancelled species to the overall species reactivity with OH remains in each case below 0.6% of the remaining terms in (17). It should be kept in mind that this simplification is valid only for relatively high initial OH concentration, in this case 4 to 5 orders of magnitude higher than the natural [OH], and for short timescale after the perturbation, typically below 100 ms. In (17) the OH lifetime τ_{OH} and its initial concentration $[OH]_0$ are measured by the pump and probe experiment [*Calpini et al.*, 1999], and the only unknown is $\sum k_{VOC}[VOC]_0$ since the measurements of $[CO]_0$, $[O_3]_0$, and $[NO_x]_0$ are easily achieved experimentally with standard trace gas detectors and have respectively known rate constants with OH. In other words, we have a first in situ estimate of the total hydrocarbon reactivity with OH, a criteria whose significance will be discussed by *Kirchner et al.* [this issue].

In order to establish the validity of this linear approximation, the results obtained for the total VOC reactivity with the RACM mechanism are compared with those based on the simplified formalism defined by (17) for a pumped OH concentration $[OH]_0 = 3 \times 10^{10}$ molecules/cm³. The total VOC reactivity is obtained with the RACM mechanism calculating explicitly each species concentration with a time resolution of 2 ms and thus having the VOC reactivity for each time step and for each atmospheric condition stated in Table 1. On the other hand, RACM is also used to simulate the OH time decay for the different atmospheric conditions. From the linear fit of the
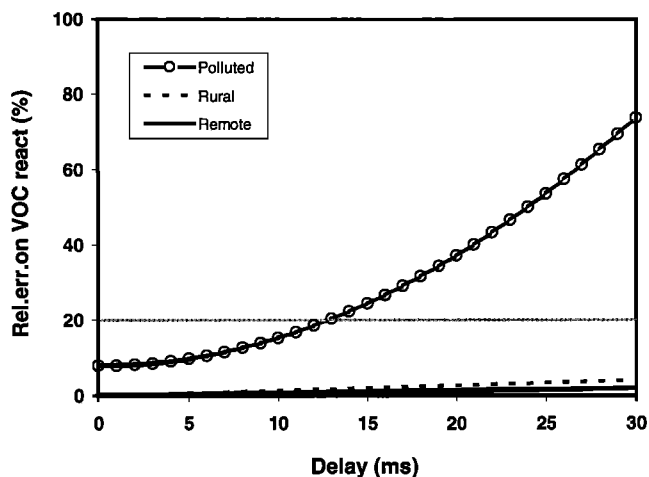
Figure 5. Relative error on the total VOC reactivity given by the simplified chemical scheme defined in (17) with respect to the reference value obtained with RACM $(1 - \Sigma k_{VOC}[VOC]_{simpl}/\Sigma k_{VOC}[VOC]_{ref})$, again for polluted, rural, and remote conditions only.

natural logarithm of this modeled OH time dependence over the first 30 ms, the OH lifetime is retrieved. By using this value with the initial concentrations of NO_x, CO, O_3, and OH in (17), the total VOC reactivity with OH based on the simplified scheme is retrieved. Figure 5 shows the relative error (%) comparing the total VOC reactivity obtained by (17) with the one calculated at each time step by RACM. The polluted case is characterized by a rapid secondary increase of OH induced by the HO_2 formation (R6) and subsequent reaction with NO (via reactions (R8) and (R3)) thus making the first-order approximation valid for shorter time delay only. Note that under the same conditions the secondary production of OH due to the ozone plus alkenes reaction is smaller by 5 orders of magnitude than the production by NO + HO_2. In the polluted case and for delays shorter than 12 ms the relative error on the VOC reactivity remains lower than 20%. For remote and rural atmospheric conditions, the OH relaxation being much slower, (17) remains valid for longer timescale. In these two latter cases the VOC reactivity is obtained with errors that are lower than 3% for a timescale of 30 ms. A similar result is obtained for the moderately polluted case (not shown here).

The relative error on the VOC reactivity was further studied in a series of runs where $[OH]_0$ was varied by 2 orders of magnitude between 10^9 to 10^{11} molecules/cm^3. In the remote case due to the presence of very reactive VOC species a difference of 20% on the total VOC reactivity was observed between (17) and the complete RACM mechanism for time delays over 50 ms.

Finally, we may consider this simplified mechanism expressing the total VOC reactivity with OH in situ with an accuracy of better than 80% compared with its value predicted by RACM. The validity of this formalism is both limited by the amount of secondary OH produced (in the case of highly polluted conditions) and the error induced by too high initial OH concentration.

So far, we have shown that the OH lifetime strongly depends on different typical air conditions, both in concentration and in time, even under timescale as short as 20 ms. Furthermore, the atmospheric chemical reactions describing the OH time decay

Table 2. Gas Concentration in the Experimental Gas Mixture[a]

Compounds	Moderately Polluted	Rural$_{NO_x}$	Rural$_{VOC}$
C_3H_6	17	10	11.6
C_4H_{10}	143.3	84.3	97.3
C_2H_4	51.2	30.1	34.8
NO	5	4	1
NO_2	148	86	2
O_3	71	80	120

[a]All values in ppb.

on short timescales can be much simplified. A pseudo first-order reaction for OH has then been confirmed as a good estimate of the complete chemical code under the particular condition of this pump and probe experiment. This formalism can be checked against experimental results obtained in a controlled environment using a flow tube reaction chamber and different types of gas mixtures with synthetic air conditions.

5. Comparison Between Predicted and Measured $\Sigma k_{VOC}[VOC]$ in Different VOC/NO$_x$ Environments

In this pump and probe experiment a gas mixture is continuously flown through the reaction cell. This synthetic air is formed of NO_x, VOCs, and O_3 added to the $Ar:O_2:H_2O$ gas stream at atmospheric pressure and temperature. VOCs are composed of propene, n-butane, and ethene in a ratio of 1:8:3 for total VOC concentrations varying between 125 and 210 ppb in accordance with atmospheric conditions reported by *Chameides et al.* [1992]. NO_x and O_3 concentrations are controlled so that three stable gas mixtures are tested with values following *Finlayson-Pitts and Pitts* [1986] for moderately polluted, rural$_{NO_x}$, and rural$_{VOC}$ conditions, respectively. The experimental concentrations are listed in Table 2. We used the term rural$_{NO_x}$ for an air parcel in rural conditions characterized by the presence of high NO_x concentrations or similar to an air pollution condition downwind from a large urban area, and rural$_{VOC}$ for a rural condition with low NO_x concentrations. Hence, for NO_x = NO + NO_2 concentrations, the experimental NO_2/NO does not exhibit a realistic ratio. This is due to the dilution bench where O_3 and NO_x are mixed together before the reaction chamber in order to assure a homogeneous gas mixture at the reaction site. As ozone reacts very fast with nitric oxide, a large fraction of NO_x at the reaction site is NO_2. For this reason, O_3 and NO_x are measured directly at the reaction site by UV differential absorption and chemiluminescence technique, respectively. The three VOC species are obtained directly from a gas calibration tank. The uncertainty on the VOC concentrations is estimated below 10%, while NO_x and O_3 gas detectors have both a precision of ±1 ppb.

The measurements were performed by time steps of 1 ms for a time delay varying from 1 to 20 ms. For each time delay the LIF signal is averaged over typically 1000 laser shots acquired on an oscilloscope. Each data point is converted to an [OH] equivalent concentration value taking into account the overall LIF detection efficiency. The pump and the probe beam diameters were set at 6 and 3 mm, respectively, and the flow speed of the synthetic air stream was 5.2 cm/s at the reaction site. The conditions (2) and (3) are fulfilled for time delays Δt_1 = 29 ms and Δt_2 = 86 ms. Therefore the measured OH relaxation for time delays below Δt_1 is obtained without per-
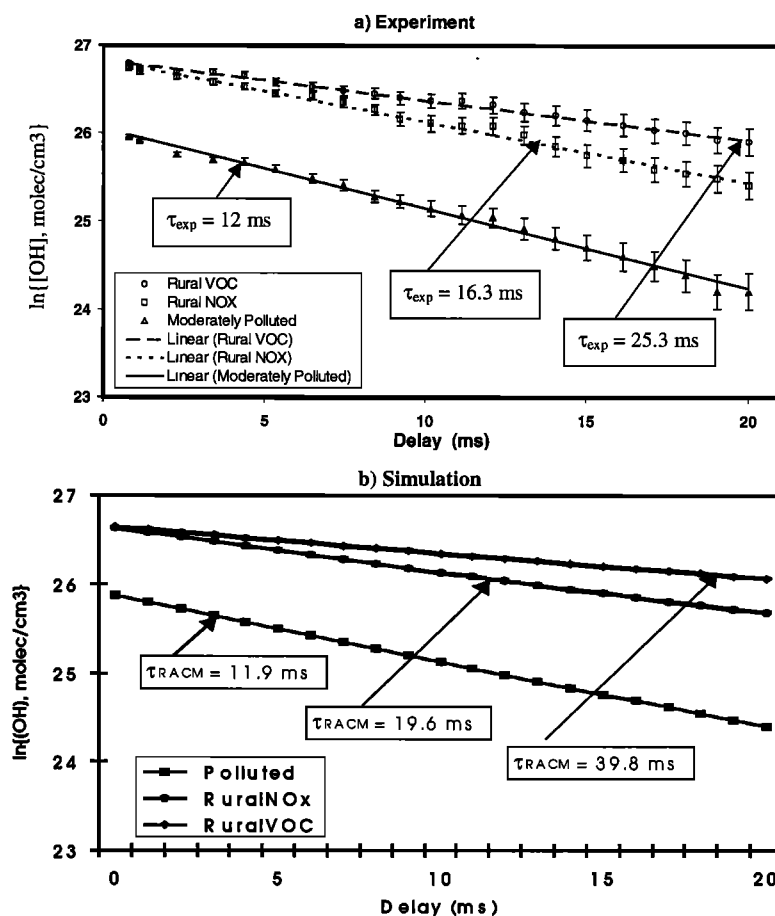
Figure 6. Natural logarithm of the pump and probe OH concentration versus time measured in the reaction cell for the three different $NO_x/VOC/O_3$ gas mixtures defined in Table 2: (a) experimental values and (b) RACM-predicted results. OH lifetimes τ are given by the slope of the linear fits. The experimental error bars represent the overall uncertainty of the statistical variability of the fluorescence signal and variations in the trace gas concentrations, assumed to be random.

turbation due to transport effect. With a pulse repetition rate of 10 Hz, no memory effect of OH can be present for $\Delta t = 100$ ms.

The experimental results are presented in Figure 6a with each data point shown with an experimental uncertainty corresponding to the uncertainties associated to the conversion from the LIF signal to the OH concentration, the statistical variability of the fluorescence signal, and the determination of the trace gas concentrations estimated at 10% and assumed to be random. For each of the three airstream conditions the time dependence of the [OH] natural logarithm is approximated by a linear fit. From this linear fit an experimental lifetime τ_{exp} for OH is obtained for each gas mixture with a value of $\tau_{exp} = 12 \pm 1.8$ ms for the moderately polluted case, 16.3 ± 3.2 ms for rural$_{NO_x}$, and 25.3 ± 6.2 ms for rural$_{VOC}$. Figure 6b presents the predicted results obtained for the same experimental conditions replacing in the RACM mechanism OLT by propene (C_3H_6), HC3 by n-butane (C_4H_{10}), and OL2 by ethene (C_2H_4). Their associated rate constants are $k_{OH} = (2.64 \pm 0.61) \times 10^{-11}$, $(2.44 \pm 0.55) \times 10^{-12}$, and $(8.54 \pm 5.86) \times 10^{-12}$ cm^3 molecules^{-1} s^{-1}, respectively. The uncertainties on the different VOC rate constants are calculated following *Atkinson* [1997]. They have a relative effect ranging from 20% for n-butane to close to 70% for ethene. From the predictive results obtained by RACM the OH lifetime τ_{RACM} is retrieved. Fi-

nally, using directly (17) with the known [rate constant times concentration] for each VOC species listed in Table 2 the reference OH lifetime τ_{ref} is retrieved from the simplified mechanism. All these results are listed in Table 3.

The agreement between experimental and simulated OH lifetimes is very good for the moderately polluted case. For the rural$_{NO_x}$ case the experimental value is 20% higher than the value calculated by the model and 12% higher than the value estimated by applying (17). Considering the error limits, there is an agreement between experiment and model. For the rural$_{VOC}$ there is a large difference between τ_{exp} on the one hand and τ_{ref} and τ_{RACM} on the other hand. However, one has to take into account also the large error limits especially of τ_{ref}. This uncertainty in τ_{ref} results only from uncertainties in the kinetic data. They affect τ_{RACM} in a similar manner so that even for the rural$_{VOC}$ case the OH lifetimes agree inside their error limits.

The uncertainties defined in Table 3 did not include errors resulting from the simplifications made for obtaining (17). To evaluate them, τ_{ref} is directly compared with τ_{RACM} using the modified RACM mechanism where (OH + OH) and the updated rate constant for reaction (HO + NO$_2$) were added. The results τ_{ref}/τ_{RACM} are presented in Table 3. The OH loss rate calculated with the modified RACM mechanism is 3–7% smaller than the results applying (17). Besides the formation of

Table 3. OH Lifetimes and VOC Reactivity for the Three Experimental Conditions

	Moderately Polluted	Rural$_{NO_x}$	Rural$_{VOC}$
τ_{exp}, ms	12 ± 1.8 ($R = 0.97$)	16.3 ± 3.2 ($R = 0.96$)	25.3 ± 6.2 ($R = 0.97$)
τ_{ref}, ms	11.5 ± 3.1	18.3 ± 4.9	36.9 ± 9.9
τ_{RACM}, ms	11.9	19.6	39.8
τ_{ref}/τ_{RACM}, %	96.9	93.3	92.8
$\sum k_{VOC}[VOC]_{exp}$, s^{-1}	26.9 ± 6.9	24.5 ± 12.5	33.1 ± 13.5
$\sum k_{VOC}[VOC]_{ref}$, s^{-1}	30.3 ± 8.2	17.8 ± 4.8	20.6 ± 5.6
$\sum k_{VOC}[VOC]_{RACM}$, s^{-1}	27.6	14.2	18.7

OH from secondary reactions, the other reason for this difference is the change in the concentration of the reactants during the experiment and in particular the OH concentration decrease itself. Replacing the OH initial concentration in (17) by the "mean" OH concentration (i.e., after 10 ms) lowers this overestimation of the OH loss using (17) to 1.5–3%. Nevertheless, in all three cases the errors caused by the simplification remained below 10%.

We may now use (17) and get directly the total VOC reactivity with OH:

$$\sum k_{VOC}[VOC]_{exp} = 1/\tau_{OH} - \sum k_{NO_x}[NO_x]_0 - k_{O_3}[O_3]_0$$
$$- 2k_{OH}[OH]_0. \tag{18}$$

The inverse of the OH lifetime $1/\tau_{OH}$ is given by the pump and probe measurement, the NO_x and O_3 concentrations are measured by chemical analyzers, and the respective OH reaction rate constants k_{NO_x}, k_{O_3}, and k_{OH} are recommended by *Atkinson et al.* [1997]. $\sum k_{VOC}[VOC]_{exp}$ is directly calculated from (18) with an overall uncertainty due to the determination of the OH lifetime, the respective reaction rates uncertainties of OH with NO_x, O_3, and OH, the 10% precision in the concentrations of $[NO_x]_0$ and $[O_3]_0$, and the 30% precision in the determination of $[OH]_0$. In the moderately polluted case, more than 80% of the error sources on $\sum k_{VOC}[VOC]_{exp}$ are due to $\sum k_{NO_x}[NO_x]_0$, while the pump and probe experimental determination of $1/\tau_{OH}$ and $2k_{OH}[OH]_0$ contributes to less than 20% of the error. In other words, the largest contribution to the error reported on $\sum k_{VOC}[VOC]_{exp}$ is in this case due to uncertainties that are not related to the pump and probe method. This figure changes in the rural$_{VOC}$ case where the term $2k_{OH}[OH]_0$ plays the major role on the $\sum k_{VOC}[VOC]_{exp}$ uncertainty. The total VOC reactivity $\sum k_{VOC}[VOC]_{ref}$ is the reference value obtained as the sum of the propene, n-butane, and ethene rate constants times their respective concentrations. The uncertainties reported in Table 3 for the three $\sum k_{VOC}[VOC]_{ref}$ values are obtained taking into account the 10% uncertainty on the different VOC concentrations and their associated uncertainty on the respective rate constant with OH. Finally, $\sum k_{VOC}[VOC]_{RACM}$ is retrieved using τ_{RACM} and (18).

Comparing the $\sum k_{VOC}[VOC]_{ref}$ and $\sum k_{VOC}[VOC]_{RACM}$ values, one can see that for all three cases the error resulting from the simplification (difference between $\sum k_{VOC}[VOC]_{ref}$ and $\sum k_{VOC}[VOC]_{RACM}$) is considerably smaller than the uncertainty in the kinetic data (error limits of $\sum k_{VOC}[VOC]_{ref}$). Estimating the uncertainty of $\sum k_{VOC}[VOC]_{RACM}$ being equal to the uncertainty of $\sum k_{VOC}[VOC]_{ref}$, there is an agreement with the experimental values inside the error limits. $\sum k_{VOC}[VOC]_{exp}$ is calculated by (18) with error limits that become larger if τ_{exp} has larger uncertainties and also if the

proportion of the OH loss by reaction with VOC gets smaller compared to the overall OH loss. In particular, in the case of high NO_x concentrations the contribution of uncertainties in the kinetic data needed in (18) to the error limits of $\sum k_{VOC}[VOC]_{exp}$ is high, for example, more than 50% in the rural$_{NO_x}$ case.

One should also mention that the actual experiment itself gives better results in highly polluted conditions where very short OH lifetimes are expected. This is partially linked to the limit of detection of the apparatus giving a lowest OH concentration detection of some 10^8 OH molecules/cm^3. In order to have a sufficient dynamic range for each of the three gas stream conditions, the experiments were performed with $[OH]_0$ slightly above the proposed domain of validity of (18), namely, with initial OH concentrations up to 3.75×10^{11} OH molecules/cm^3 for the rural$_{VOC}$ case. In this case the linearization errors defined in section 3 are larger with the most important effect for the longer OH lifetimes. In addition, the time window of 20 ms was set so to fulfill the condition of a "pure chemical regime" (no transport effect due to the gas flow). However, this time window appeared to be short especially for the detection of OH lifetime above typically 30 ms as is the case for the rural$_{VOC}$ case.

Finally, it is important to underline that the experiments were performed with different NO_2/NO ratios higher than what is the case in the real atmospheric environment. Reaction (R3) ($HO_2 + NO \rightarrow OH + NO_2$) being an important source of secondary OH formation and the experiments being performed with low NO concentration (due to its rapid reaction with ozone in the dilution bench and conversion to NO_2), no secondary OH was perturbing τ_{exp} in this case. Nevertheless, this secondary OH formation could eventually have had a strong impact on the OH lifetime if the experiments were performed under more realistic NO_2/NO ratios. In order to address this problem, box model runs with RACM were repeated for the moderately polluted case keeping any conditions similar to the experiment, except the NO_2/NO ratio changed to 350 ppb/150 ppb. However, even in this case, no significant secondary OH formation was predicted during the first 20 ms.

6. Conclusion

With an in situ "pumped" OH concentration obtained by O_3 flash photolysis, the OH time relaxation can be used to obtain a first estimate of the total volatile organic compound reactivity with OH in the atmosphere. This OH time decay is approximated for short time delays by a simplified chemical system. On the one hand, the interference due to transport by the wind and diffusion is avoided adapting the repetition rate and beam geometry of the experiment. On the other hand, the only significant chemical processes governing the OH loss are the

radical reactions with VOCs, NO_x, O_3, CO, and OH itself. Therefore a first in situ estimate of the total VOC reactivity with OH $\Sigma k_{VOC}[VOC]$ can be obtained measuring the pumped OH concentration $[OH]_0$ at $t = 0$ and the inverse OH lifetime with the pump and probe experiment, with additional measurements of NO_x, CO, and O_3 concentrations by standard trace gas detectors. Under these conditions a simple scheme was defined that gives $\Sigma k_{VOC}[VOC]$ with an uncertainty smaller than 20% with respect to the RACM chemical mechanism for an OH decay time below 12 ms in a highly polluted case, while in less polluted conditions a better accuracy is obtained even for longer delays.

On the basis of this analysis a series of pump and probe OH measurements were performed in a controlled environment with gas mixtures that were comparable to three different levels of pollution. In the case of a polluted environment the pump and probe OH experiment gave an estimate of the experimental $\Sigma k_{VOC}[VOC]_{exp}$ in good agreement with the referenced value $\Sigma k_{VOC}[VOC]_{ref}$ calculated directly as the sum of the VOC species in the gas stream times their respective rate constant with OH. The associated uncertainty was in large part due to the poorly known rate constant of NO_x with OH rather than the method itself. This result was confirmed by $\Sigma k_{VOC}[VOC]_{RACM}$ obtained from the complete RACM mechanism. For more rural-like experimental conditions, while the different results were still in accordance (within the error limits), both the chemistry with secondary OH interference and the apparatus with its actual OH detection limit were limiting the final accuracy of the results.

The upgrade of the experimental layout will consist first of using a Kr excimer laser for the ozone photodissociation. A higher ozone absorption efficiency will be gained at 248 nm, together with a higher energy per pulse (600 mJ) and a wider beam size (typically 10 × 25 mm without beam expander). The latter point is of importance since it will assure a "pure chemical regime" (no transport effect) over longer timescales. Furthermore, the OH detection will be performed with a gated photodetector and a LIF laser source tuned around 308 nm. This will essentially prevent the experiment from any secondary OH formation due to the probe laser beam itself. With these changes an OH detection limit of the order of 10^6 to 10^7 OH molecules/cm^3 is expected thus giving the chance for pump and probe OH measurements performed at much lower initial OH concentration (typically below 10^{10} OH molecules/cm^3). The pump and probe technique will also be applied as a remote sensing technique (lidar configuration).

$\Sigma k_{VOC}[VOC]$ is the reactivity-weighted sum of all the different volatile organic compounds and shall give an important new criterion for our understanding of the control of the ozone formation in a photochemical smog. A companion paper by Kirchner et al. [this issue] shows in detail what can be gained with these new experimental parameters measured in atmospheric conditions.

References

Atkinson, R., Gas-phase tropospheric chemistry of volatile organic compounds, 1, Alkanes and alkenes, *J. Phys. Chem. Ref. Data*, 26(2), 215–290, 1997.

Atkinson, R., D. L. Baulch, R. A. Cox, R. F. Hampson Jr., J. A. Kerr, M. J. Rossi, and J. Troe, Evaluated kinetic and photochemical data for atmospheric chemistry: Supplement VI, *J. Phys. Chem. Ref. Data*, 26(2), 521–1011, 1997.

Brock, J. C., and R. T. Watson, Ozone photolysis: Determination of the $O(^3P)$ quantum yield at 266 nm, *Chem. Phys. Lett.*, 71, 371–378, 1980.

Brune, W. H., et al., Airborne in situ OH and HO_2 observations in the cloud-free troposphere and lower stratosphere during SUCCESS, *Geophys. Res. Lett.*, 25, 1701–1704, 1998.

Calpini, B., Air pollution: Measuring techniques and impact on our environment, *Analusis*, 27(4), 291–301, 1999.

Calpini, B., F. Jeanneret, M. Bourqui, A. Clappier, R. Vajtai, and H. van den Bergh, Direct measurement of the total reaction rate of OH in the atmosphere, *Analusis*, 27(4), 328–336, 1999.

Chameides, W. L., et al., Ozone precursor relationships in the ambient atmosphere, *J. Geophys. Res.*, 97, 6037–6055, 1992.

Derwent, R. G., and M. E. Jenkin, Hydrocarbons and the long range transport of ozone and PAN across Europe, *Atmos. Environ., Part A*, 25, 1661–1678, 1991.

Ehhalt, D. H., F. Rohrer, A. Wahner, M. J. Prather, and D. R. Blake, On the use of hydrocarbons for the determination of the tropospheric OH concentrations, *J. Geophys. Res.*, 103, 18,981–18,997, 1998.

Fehsenfeld, F., et al., Emissions of volatile organic compounds from vegetation and the implications for atmospheric chemistry, *Global Biogeochem. Cycles*, 6, 389–430, 1992.

Finlayson-Pitts, B. J., and J. N. Pitts, *Atmospheric Chemistry: Fundamentals and Experimental Techniques*, Wiley-Interscience, New York, 1986.

Fuhrer, J., and P. Bungener, Effects of air pollutants on plants, *Analusis*, 27(4), 355–360, 1999.

Gong, W., and H.-R. Cho, A numerical scheme for the integration of the gas phase chemical rate equations in 3-D atmospheric models, *Atmos. Environ.*, 27, 2147–2160, 1993.

Kirchner, F., F. Jeanneret, A. Clappier, B. C. Krüger, H. van den Bergh, and B. Calpini, Total VOC reactivity in the planetary boundary layer, 2, A new indicator for determining the sensitivity of the ozone production to VOC and NO_x, *J. Geophys. Res.*, this issue.

Kuhn, M., et al., Intercomparison of the gas-phase chemistry in several chemistry and transport models, *Atmos. Environ.*, 32, 693–709, 1998.

Mauldin, R. L., III, D. J. Tanner, and F. L. Eisele, Measurements of OH during PEM-Tropics A, *J. Geophys. Res.*, 104, 5817–5827, 1999.

Molina, L. T., and M. J. Molina, Absolute absorption cross section of ozone in the 185- to 350-nm wavelength range, *J. Geophys. Res.*, 91, 14,501–14,514, 1986.

Neftel, A., Examples of the importance of trace gas measurements in the Milan ozone plume, *Analusis*, 27(4), 325–327, 1999.

Paulsen, S. E., M. Chung, A. D. Sen, and G. Orzechowska, Measurement of OH radical formation from the reaction of ozone with several biogenic alkenes, *J. Geophys. Res.*, 103, 25,533–25,539, 1998.

Seinfeld, J. H., and S. N. Pandis, *Atmospheric Chemistry and Physics: From Air Pollution to Climate Change*, Wiley-Interscience, New York, 1998.

Staffelbach, T., et al., Photochemical oxidant formation over southern Switzerland, 1, Results from summer 1994, *J. Geophys. Res.*, 102, 23,345–23,362, 1997.

Stockwell, W. R., P. Middleton, J. S. Chang, and X. Tang, The second generation Regional Acid Rain Model chemical mechanism for regional air quality modeling, *J. Geophys. Res.*, 95, 16,343–16,367, 1990.

Stockwell, W. R., F. Kirchner, M. Kuhn, and S. Seefeld, A new mechanism for regional atmospheric chemistry modeling, *J. Geophys. Res.*, 102, 25,847–25,879, 1997.

B. Calpini (corresponding author), A. Clappier, F. Jeanneret, F. Kirchner, and H. van den Bergh, Air Pollution Laboratory (LPA), Swiss Federal Institute of Technology (EPFL), 1015 Lausanne, Switzerland. (bertrand.calpini@epfl.ch)